Electronic Supplementary Information (ESI):

Dewetting Transitions Couple to K-channel Activation in Cytochrome c Oxidase

Shreyas Supekar and Ville R. I. Kaila[*]

Department Chemie, Technische Universität München, Lichtenbergstraße 4, D-85748 Garching, Germany.
[*]ville.kaila@ch.tum.de

Methods

Molecular dynamics (MD) simulations

The MD simulations were based on the X-ray structure of bovine CcO[1] (PDB ID: 1V54). Subunits I and II of CcO were embedded in a 1-palmitoyl-2-oleoyl-sn-glycero-3-phosphocholine (POPC) membrane, solvated with TIP3P water molecules, and a 100 mM NaCl concentration (29 Na$^+$, 10 Cl$^-$), comprising in total *ca.* 88,840 atoms. Residues Glu-242 and Asp-364 of subunit I were modeled in their protonated states, with Glu-242 flipped "up" towards the non-polar active site.[2] Lys-319 was modeled in both protonated and deprotonated states. Heme a was modeled in the oxidized state, and the BNC in the P$_M$ (a_3^{IV}=O^{2-}/Cu^{II}-OH$^-$/Tyr-O·), P$_R$ (a_3^{IV}=O^{2-}/Cu^{II}-OH$^-$/Tyr-O$^-$), O$_H$ (a_3^{III}-OH$^-$/Cu^{II}-OH$_2$/Tyr-O-) and O$_{H,R}$ (a_3^{III}-OH$^-$/Cu^I-OH$_2$/Tyr-O$^-$) states, based on DFT parameterization of the redox sites and further in-house parameterization for O$_{H,R}$ state.[3] We performed 500 ns MD simulations for P$_M$, P$_R$, O$_H$ and O$_{H,R}$ states using the CHARMM36 force field,[4] at T=310 K, with a 2 fs integration step, and Particle Mesh Ewald treatment for long-range electrostatics. In addition, 100 ns MD simulations of F$_R$ state (a_3^{III}-OH$^-$/Cu^{II}-OH$^-$/Tyr-O$^-$) were also performed based on the using the same methodology. The MD simulations were performed with NAMD 2.9-2.12 using VMD for visualization.[5,6]

Evaluation of longest connectivity along the shortest pathway (ζ)

The longest protonic connectivity along the shortest connecting path, ζ, was evaluated in order to quantify the rate-limiting distance along a Grotthuss-like proton transfer process, typical to proton transfer processes in proteins.[7] Such proton transfer processes between proton donors and acceptors are mediated by intermediate species, typically water molecules, which provide protonic connectivities for shuttling of protons. The ζ values for a given configuration can thus provide insight into the kinetic feasibility of proton transfer processes. The shortest path can be considered as the kinetically favored path for transferring a proton, whereas the longest connectivity along the shortest path would signify the rate-limiting element for the proton transfer reaction.

ζ was evaluated using a single-source single-sink variant of Dijkstra's algorithm from graph theory (Figure S14). The graph is initialized with proton donating species modeled as the source and the proton acceptor as the sink, and heavy atoms (oxygen and nitrogen atoms covalently bonded to a hydrogen atom) of the intermediate sites, which can provide protonic connectivity in the broad spatial vicinity, as the intermediate nodes. The algorithm then searches for the shortest path connecting the source to the sink. Once the algorithm reaches the sink node, ζ, the longest connectivity is obtained by walking back from the sink to source along the evaluated shortest path. The graph was constructed by optimizing node connections incrementally, starting with lower edge distances for connecting nodes to prefer low ζ-values with incremental relaxation of the edge condition before each evaluation of the shortest path.

pK_a calculations

Continuum electrostatics calculations were performed to estimate the pK_a of Lys-319 residue based on the structures from the MD simulations by solving the linearized Poisson-Boltzmann (PB) equation with MEAD.[8] Monte-Carlo pH titrations were performed using Karlsberg.[9] The calculations were based on MD snapshots every 5 ns from the 500 ns MD simulations of the P_M, P_R, O_H and $O_{H,R}$ states with Lys-319 in its protonated form. The lipids were modeled as a dielectric slab with $\varepsilon = 2$. Water molecules were also modeled with $\varepsilon = 80$. The protein structure was embedded in $\varepsilon = 4$ and was modeled explicitly.

K-channel volume calculations

The accessible volume in the K-channel was evaluated for the 500 ns MD trajectories of the P_M, P_R, O_H, and $O_{H,R}$ states. The volume was evaluated for snapshots at each ns along the trajectory for each catalytic intermediate. Lipids, water and ions were removed from the snapshots for volume evaluations. The calculations were performed using HOLLOW.[10] A cylindrical grid of dummy atoms with an atomic radius of 0.5 Å was generated to encompass the K-channel region, *i.e.*, here modeled as the space in between helices VIII, IX, X, XI from subunit-I and helix II from subunit-II, with a cylinder with a radius of 9 Å. The cylinder was placed at the Cα of Leu-288, located one helix turn above Tyr-244, and extended along the Cα of Thr-326, situated close to K-channel opening towards the solution phase. Dummy atoms outside the protein and those overlaying the protein atoms for the snapshot were removed, and the accessible volume was calculated for the remaining dummy atoms from the cylindrical grid.

Quantum chemical cluster models

Quantum chemical cluster models were constructed based on MD simulations with $\zeta < 2.5$ Å to estimate the energetics of the proton transfer from Lys-319 to Tyr-244 in the P_R and $O_{H,R}$ states. The models comprised *ca*. 220-230 atoms and the starting structures were based on the relaxed MD structure of the respective P_R and $O_{H,R}$ states. The models

included heme a_3 (without the propionic groups), Cu_B, and Tyr-244, His-290, His-291, His-240, His-376, Thr-316 and Lys-319, as well as 17-20 water molecules, which completed the hydrogen-bonded network. The cluster models were also constructed for the P_R and $O_{H,R}$ states without Lys-319 and the hydrogen-bonded water network leading to BNC to estimate intrinsic proton affinities of the three protonable sites in the BNC: Tyr-244, Cu_B and heme a_3. The energy differences were computed for the cluster models with or without a proton at the BNC, and the proton affinities for the respective was estimated by adding the energy of an extra proton in the protein environment as 276 kcal mol^{-1} (Table S1). The amino acids were cut at $C\beta$ positions, which were fixed during structure optimization at BP86-D3 level[11-13] using the multipole accelerated resolution of identity approximation (RI-MARIJ),[14] the m4 integration grid, and def2-SVP/def2-TZVP (Fe, Cu) basis sets.[15] The protein environment was modeled using a polarizable dielectric medium with a dielectric constant set to 4 using the COSMO model.[16] Single point energy calculations of the optimized structures were performed using the B3LYP-D3 functional,[17] with def2-TZVP basis sets [15]. The DFT calculations were performed with TURBOMOLE 6.6-7.1.[18]

QM/MM MD simulations

Hybrid quantum mechanics/molecular mechanics (QM/MM) calculations were performed based on the MD relaxed structures of the P_R and $O_{H,R}$ states. For proton transfer processes from Lys-319→Tyr-244, the QM region constituted of *ca*. 120-130 atoms, included the Cu_B center, residues Tyr-244, His-290, His-291, His-240, His-376, Thr-316 and Lys-319, and 11-13 surrounding water molecules forming a hydrogen-bonded network. For processes involving Glu-242→Cu_B proton transfer, the QM region comprising *ca*. 100 atoms, including the Cu_B center, residues Glu-242, Tyr-244, His-290, His-291, His-240, His-376, and 11 surrounding water molecules. The QM region was described at the BP86-D3/MARIJ level[11-14] and def2-SVP/def2-TZVP (Fe, Cu) basis sets,[15] and link atoms were introduced between the $C\alpha$-$C\beta$ atoms. The remaining system comprising *ca*. 88,700 atoms was treated classically with CHARMM36 force field.[4] The CHARMM/TURBOMOLE interface was employed for all QM/MM calculations.[19]

QM/MM reaction path optimizations were performed to evaluate proton transfer energetics from Glu-242→Cu_B in the P_R state and Lys-319→Tyr-244 in the P_R and $O_{H,R}$ states based on MD structures with ζ<2.5 Å for the respective paths and redox states. To sample the proton transfer path, the structures were subjected to harmonic restraints based on linear combination of all water O-H bond-distances between Glu-242 and Cu_B, and Lys-319 and Tyr-244 with a force constant of $k = 500$ kcal mol^{-1} Å^{-2} (Figure S12).

The QM/MM MD umbrella sampling (QM/MM MD US) simulations were initiated from the optimized QM/MM reaction paths for the P_R and $O_{H,R}$ redox states. For the QM/MM MD US simulations (Figure 4, Figure S13), we employed harmonic potentials force constant of $k = 100$ kcal mol^{-1} Å^{-2} of along the reaction coordinate obtained from reaction path optimizations using an integration step of 1 fs. The PMFs were obtained using the weighted histogram analysis method (WHAM)[20] with a convergence tolerance of 0.0001 kcal mol^{-1}.
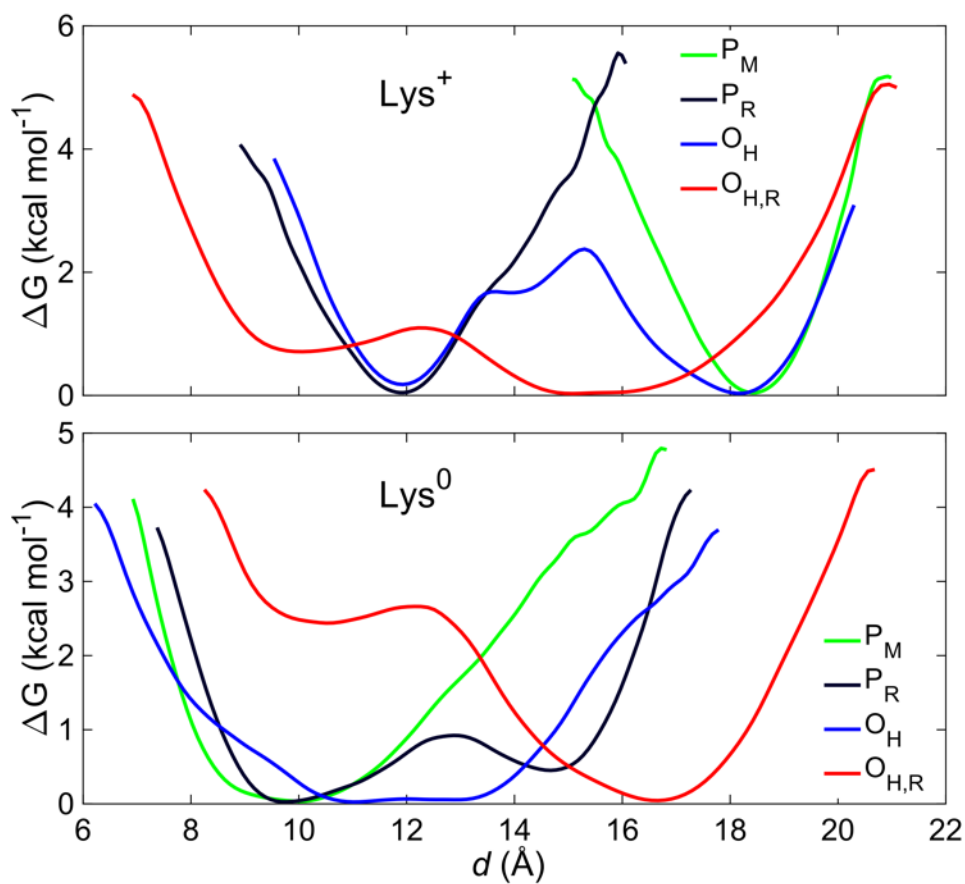
Figure S1. Free energy estimation for the "up"/"down" conformational space of Lys-319 in its protonated and deprotonated forms in the P_M, P_R, O_H and $O_{H,R}$ states based on 500 ns MD simulations.
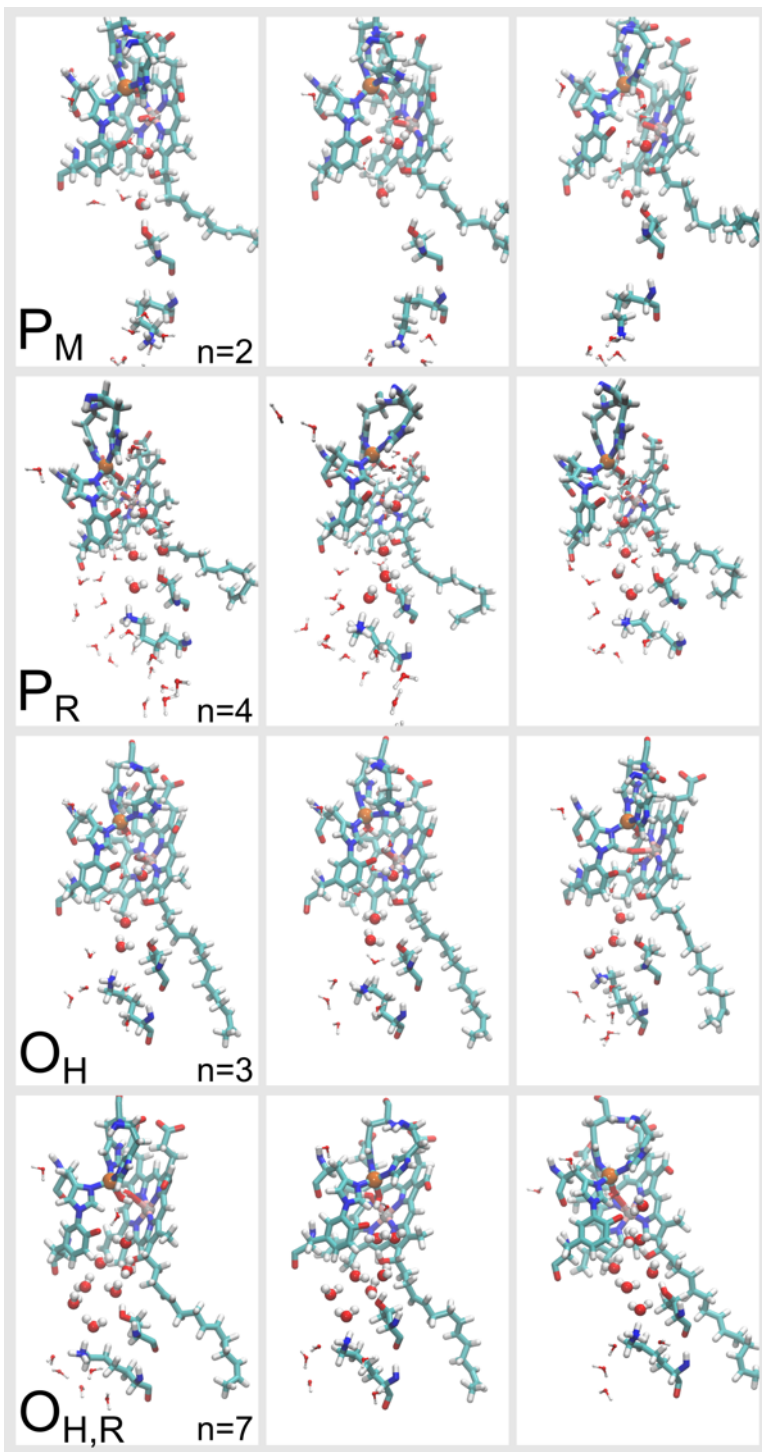
Figure S2. Snapshots from MD simulations of typical water configurations in the K-channel for the P_M, P_R, O_H and $O_{H,R}$ states. The snapshots show the most frequent water occupancies (modes) in the water occupancy distributions (dotted lines in Figure 2B) for each state.
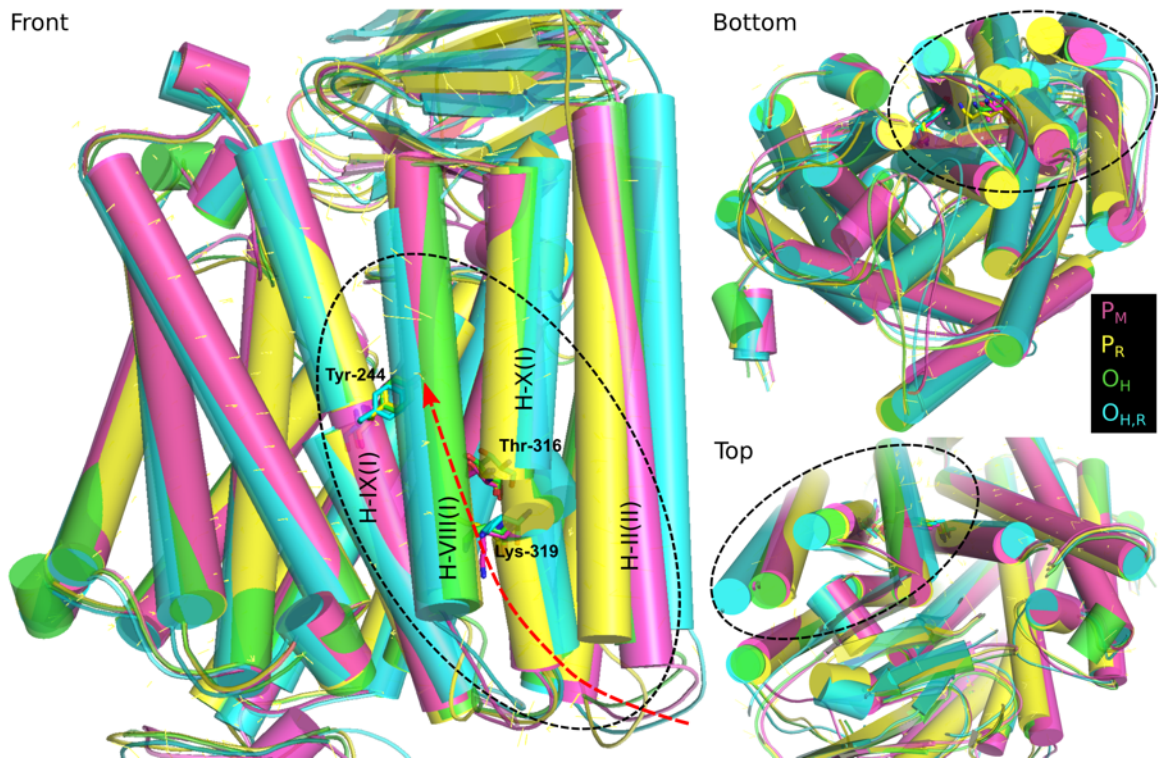
Figure S3. Averaged structures from 500 ns MD simulations of the P_M, P_R, O_H and $O_{H,R}$ states with Lys-319 modeled in its protonated form. Helices VIII, IX, and X from subunit-I and helix II from subunit-II that surround the K-channel, show structural change in the respective states. The structural change is prominent in the P→O transition.
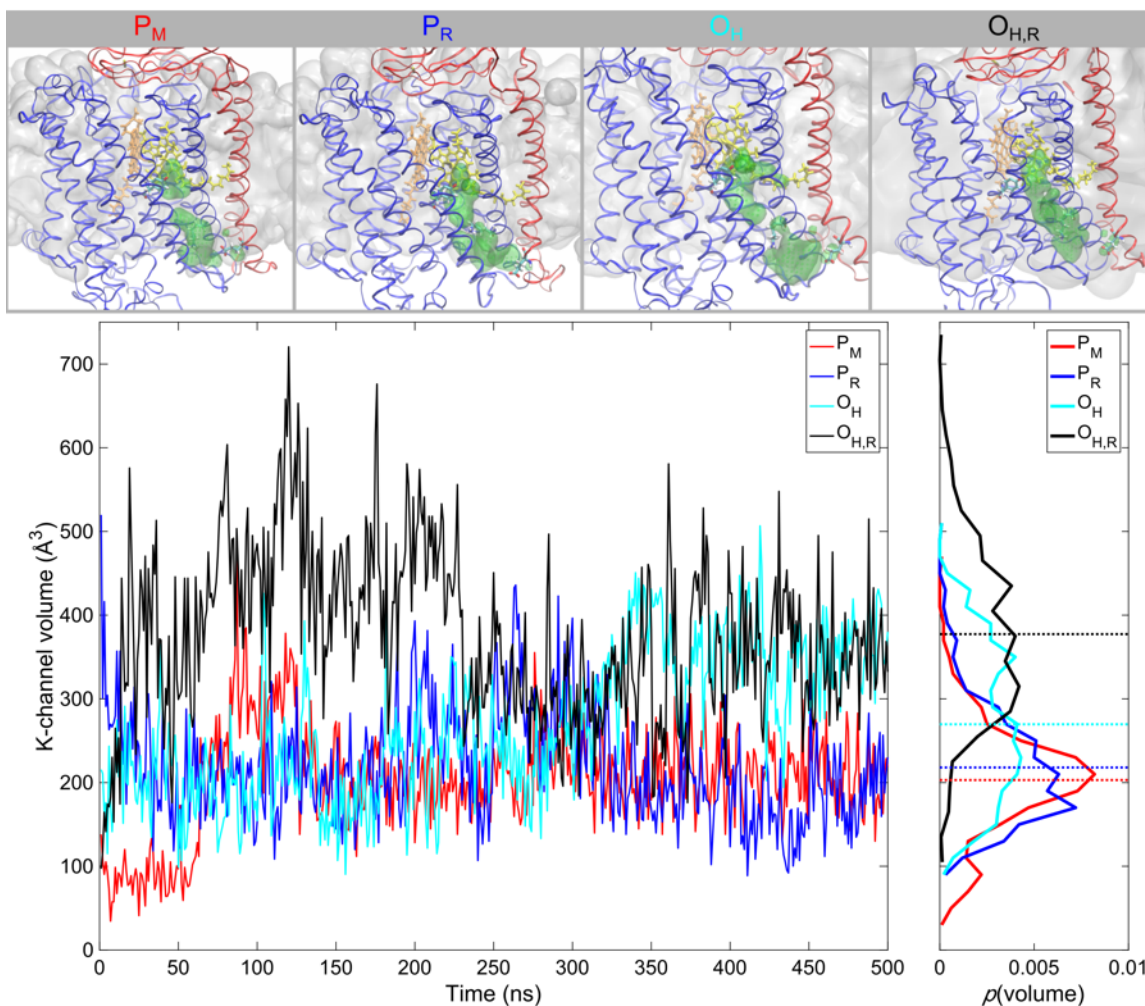
Figure S4. K-channel accessible volume in the region encapsulated by helices VIII, IX, X and XI from subunit-I and helix II from subunit-II. Left panel shows the time evolution of the accessible volume in the K-channel for the P_M, P_R, O_H and $O_{H,R}$ states. The right panel shows the probability density profiles of the volume for the respective states. Dotted lines indicate the mean accessible volume for each state. *Top*: Volume representations (in green) from typical snapshots for each state, which qualitatively reflect the mean accessible volumes (dotted lines in right panel). The volume profiles show structural changes in the O_H and $O_{H,R}$ states that lead to widening of the K-channel leading and a higher influx of water molecules. The widening of the K-channel might also be partially responsible for lowering of the Lys-319 "up"/"down" flipping barrier due to more space for the conformational transition, in an otherwise compactly packed helical region as seen in the X-ray crystal structures.
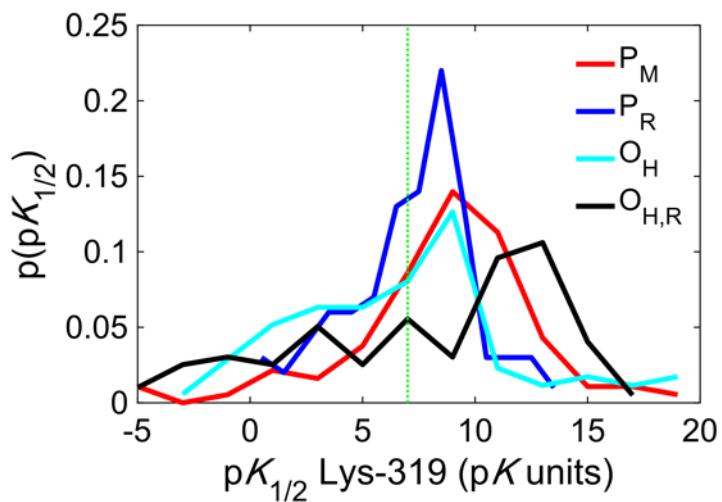
Figure S5. pK_a of Lys-319 residue obtained from Poisson-Boltzmann (PB) continuum electrostatics calculations with Monte Carlo (MC) sampling using structures at every 5 ns from 500 ns MD trajectories of the P$_M$, P$_R$, O$_H$ and O$_{H,R}$ states with Lys-319 modeled in its protonated form. The dotted green line indicates pH=7.
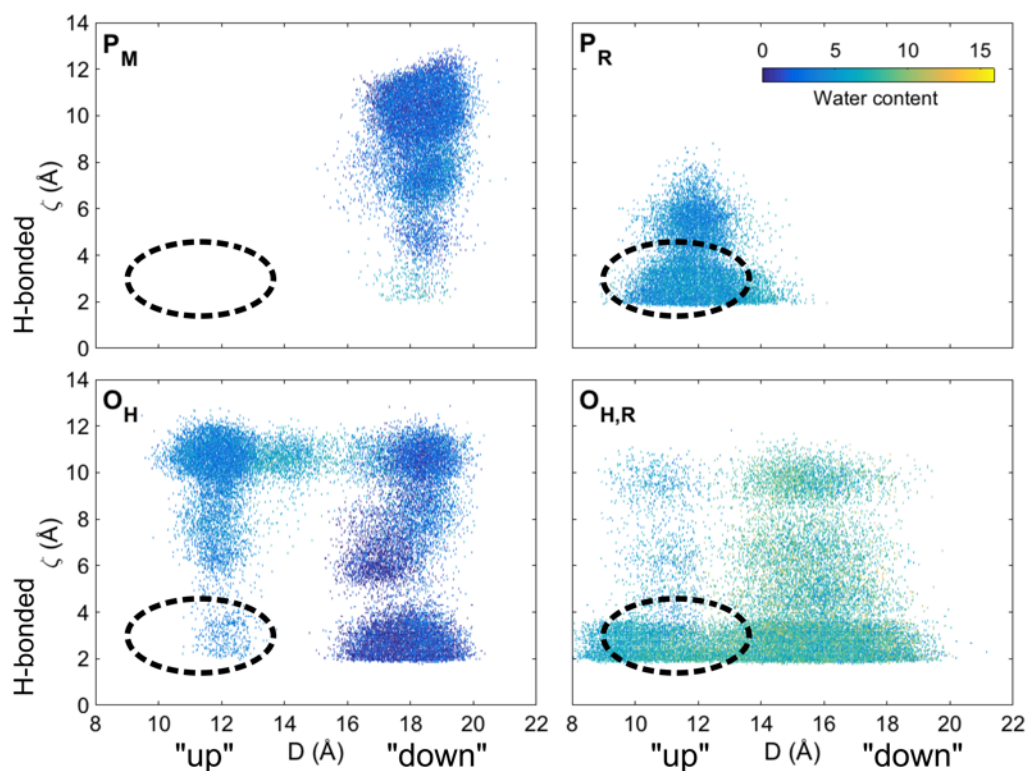
Figure S6. Lys-319 headgroup distance from Tyr-244 versus ζ values, color-coded by water occupancy from 500 ns MD trajectories of the P_M, P_R, O_H and $O_{H,R}$ states with Lys-319 in its protonated form. Each data point reflects the three observables as a function of simulation time for each state. The scatter for O_H state profile shows that the peak obtained for low ζ values ($\zeta < 2.5$ Å; hydrogen-bonded connectivity) in Figure 3B is predominantly when Lys-319 faces down towards the N-side, away from Tyr-244. Such structures would might thus be kinetically disfavored to transfer a proton from Lys-319 to Tyr-244. Dotted circles indicate configurations with Lys-319 flipped "up", and the latter forms a hydrogen-bonded protonic connectivity to Tyr-244.
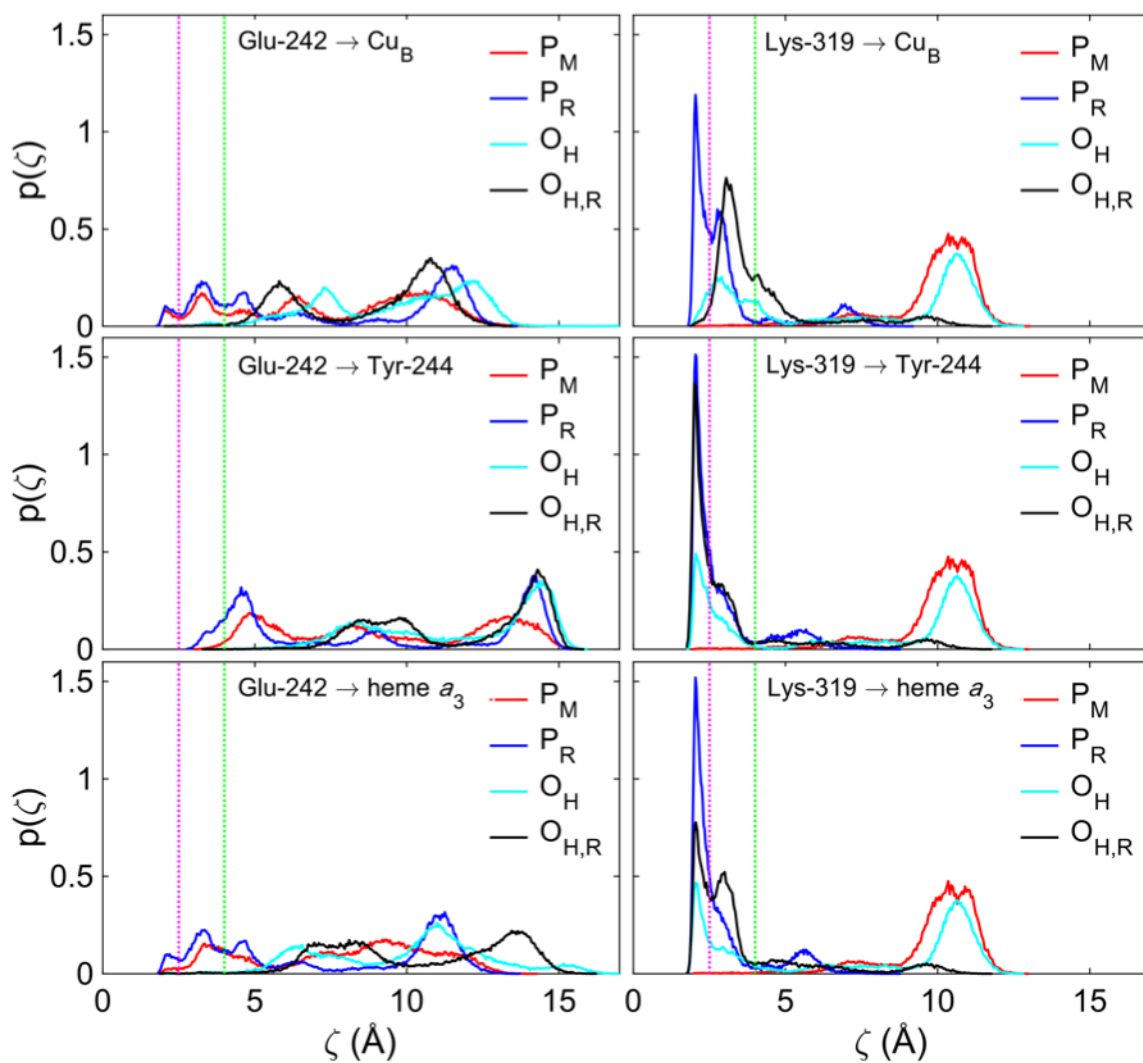
Figure S7. Longest connectivity along the shortest paths connecting the proton donor and proton acceptor, ζ, for the 500 ns MD simulations of the P_M, P_R, O_H and $O_{H,R}$ states with Lys-319 modeled in its protonated form. The ζ profiles were evaluated between of proton transfer paths between Glu-242/Lys-319 and Cu_B/Tyr-244/heme a_3.
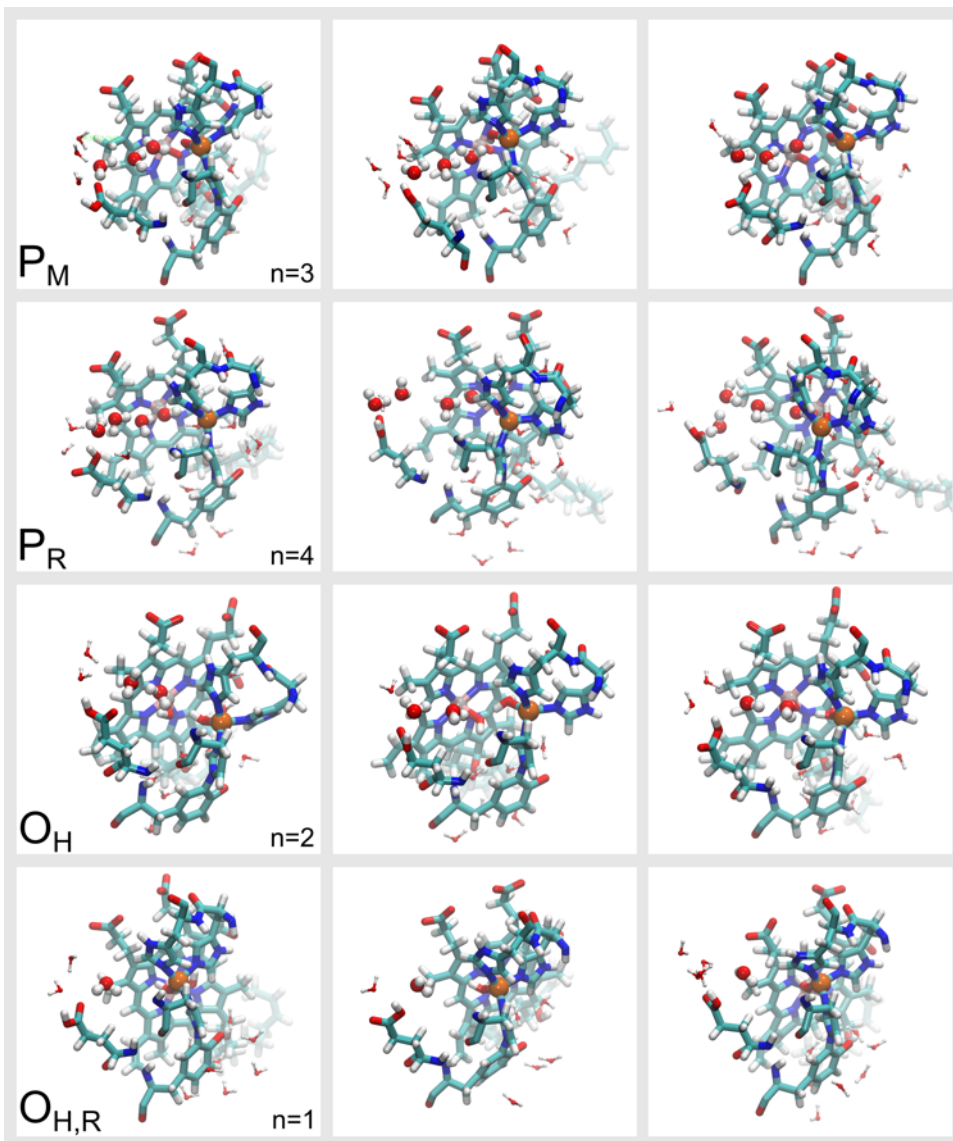
Figure S8. Snapshots from MD simulations of the P_M, P_R, O_H and $O_{H,R}$ states of typical water configurations in the non-polar cavity above the Glu-242, leading to BNC. The snapshots are representative of most frequent water occupancies (modes) in the water occupancy distributions (dotted lines in Figure 3C) for each state.
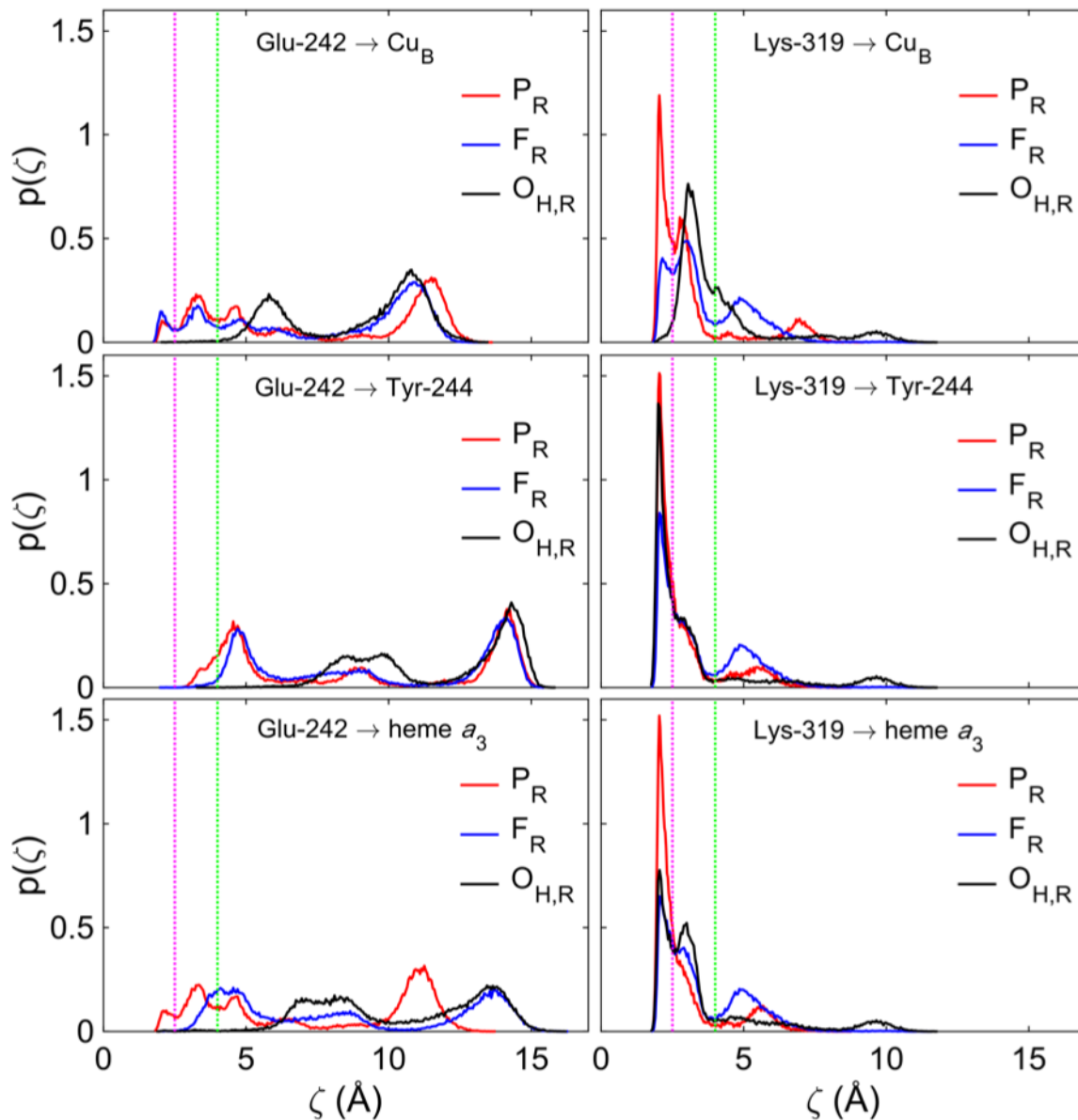
Figure S9. Longest connectivity along the shortest path connecting the proton donor and proton acceptor, ζ, for the MD simulations of the catalytic states with reduced BNC (P_R, F_R and $O_{H,R}$) states with Lys-319 modeled in its protonated form. The ζ profiles were evaluated between of proton transfer paths between Glu-242/Lys-319 and Cu_B/Tyr-244/heme a_3.
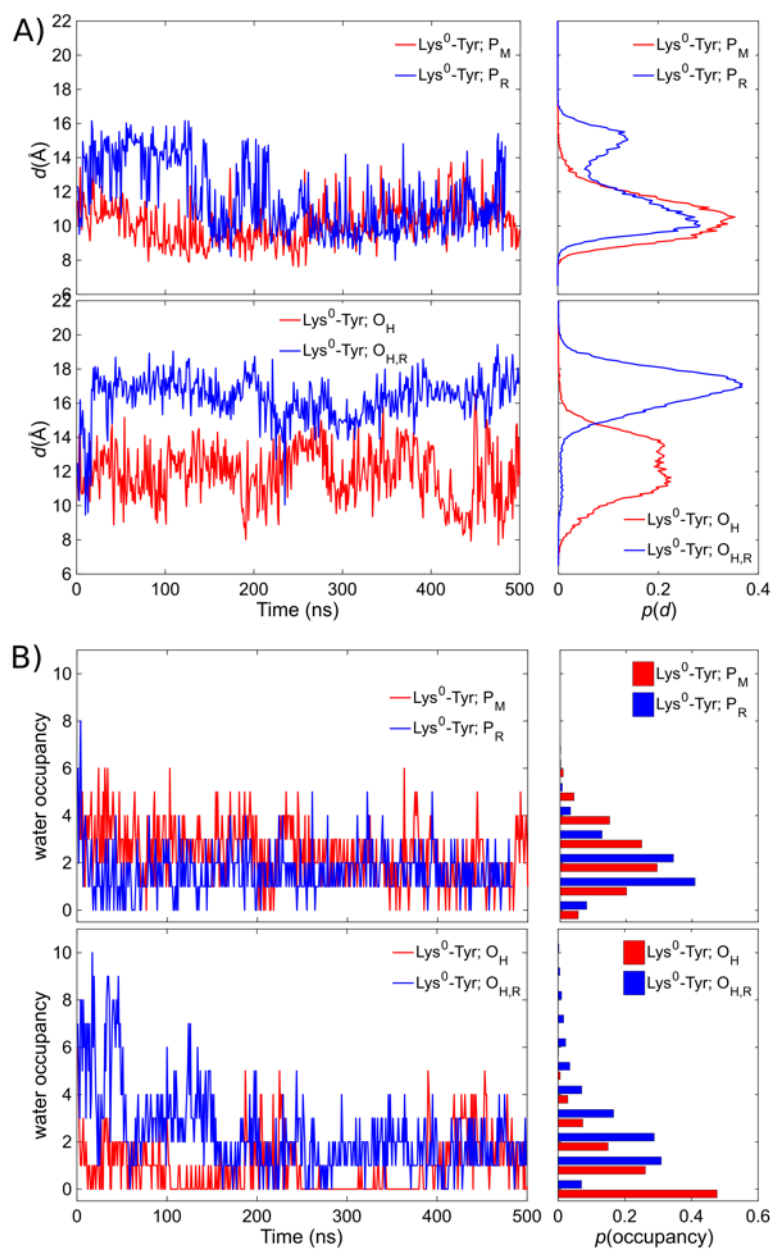
Figure S10. Dynamics of the Lys-319 sidechain and water content of the K-channel from 500 ns of MD simulations of the P_M, P_R, O_H and $O_{H,R}$ states with Lys-319 in its deprotonated form. A) The neutral Lys-319 flips "down" towards the N-side of the membrane in the one-electron reduced states, P_R and $O_{H,R}$, whereas there is an increased population in the "up"-flipped Lys in the P_M and O_H states. B) A strong reduction of the K-channel hydration across all the states, relative to respective simulations with Lys-319 modeled in its protonated form.
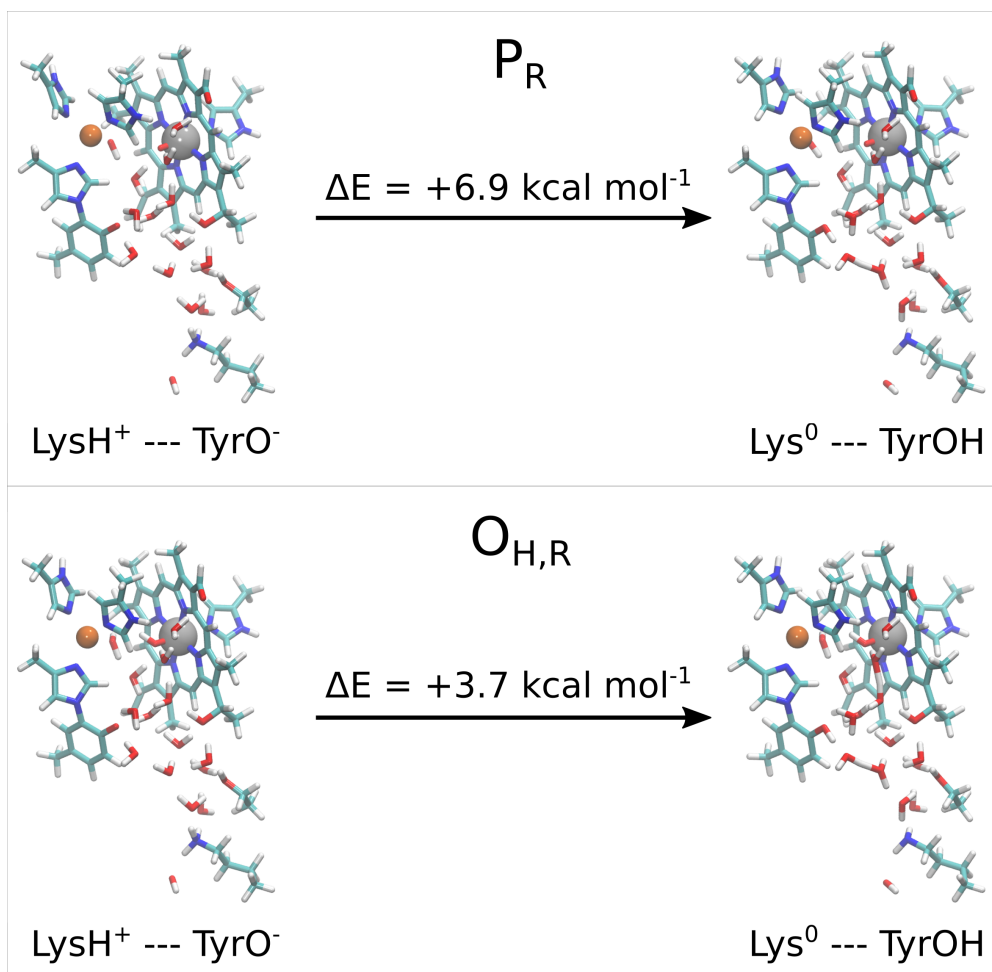
Figure S11. Quantum chemical (DFT) cluster models were employed to evaluate the energetics of proton transfer from Lys-319 to Tyr-244 in the P_R and $O_{H,R}$ states. The structures were optimized at BP86-D3/def2-SVP/def2-TZVP(Cu, Fe)/ε=4 level and the final energies were obtained from single point calculations at B3LYP-D3/def2-TZVP/ε=4 level.
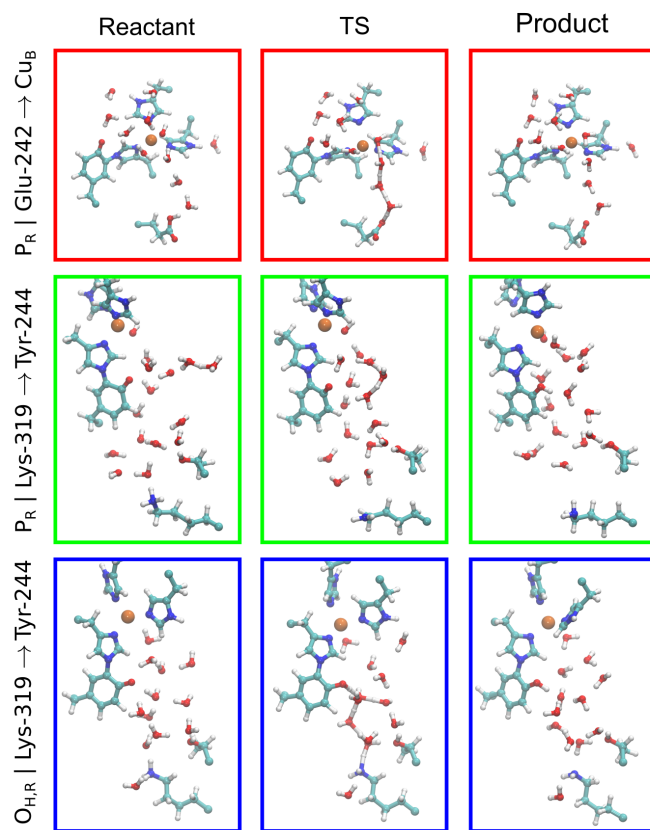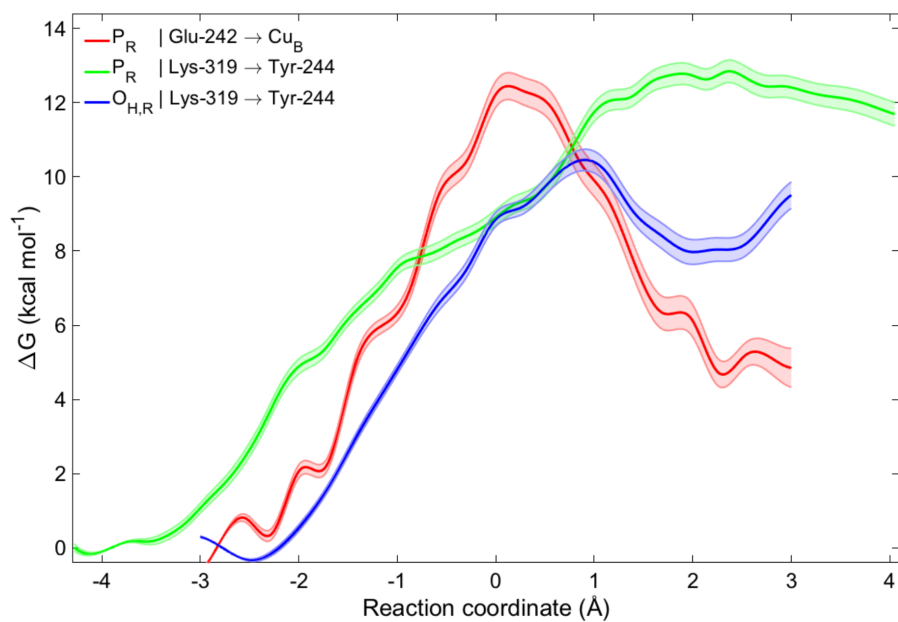
Figure S12. QM/MM-MD free energy profiles for proton transfer from Glu-242 to Cu_B in P_R state and from Lys-319 to Tyr-244 in P_R and $O_{H,R}$ states. Lighter traces indicate the error bounds for the free energy profile. Snapshots of the reactants, transition states (TS) and products for the proton transfer profiles from Glu-242 to Cu_B in P_R state and from Lys-319 to Tyr-244 in the P_R and $O_{H,R}$ state shown in the bottom panel.
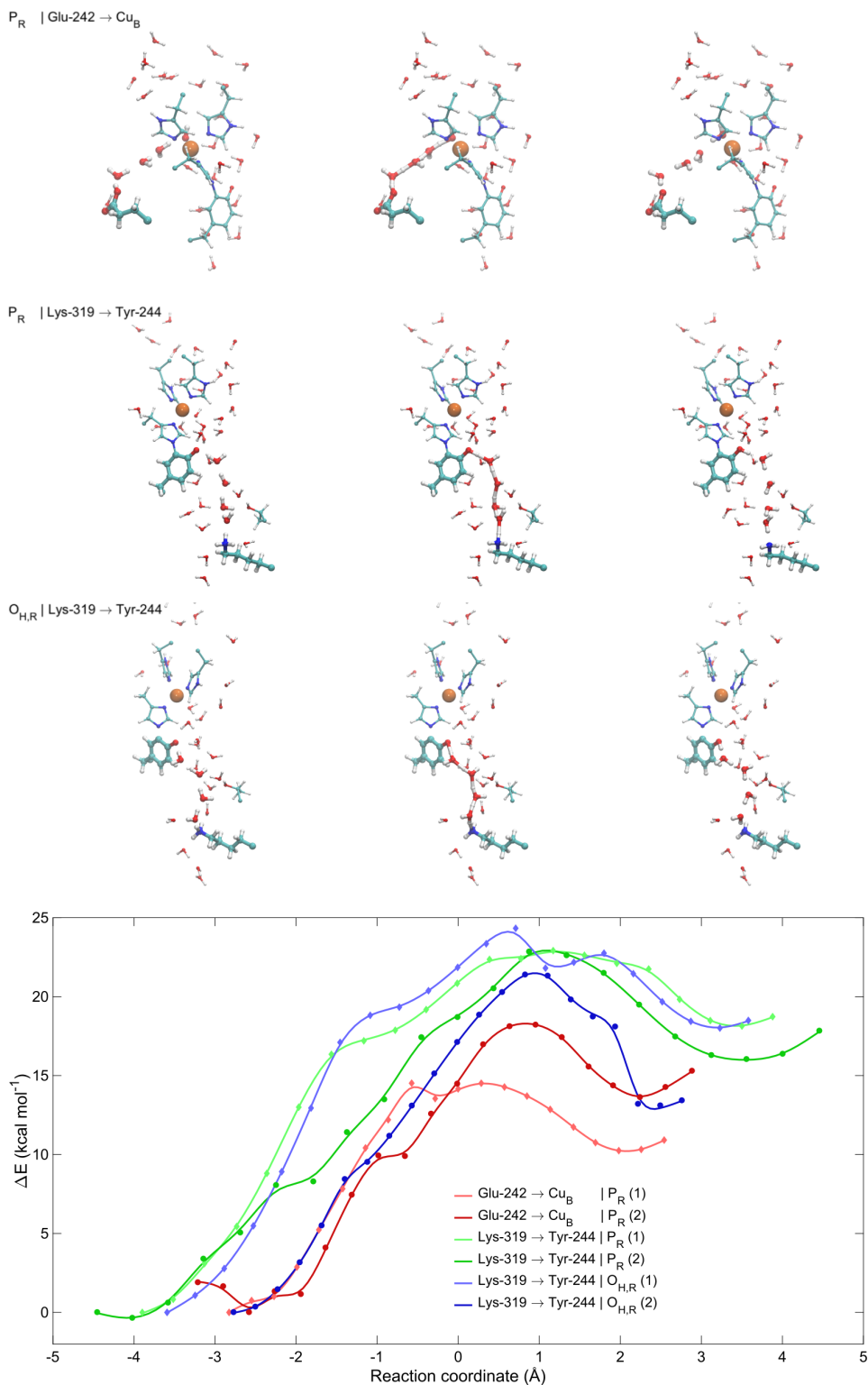
Figure S13. QM/MM reaction path optimizations for proton transfer from Glu-242 to Cu_B in P_R state and from Lys-319 to Tyr-244 in P_R and $O_{H,R}$ states. Optimized reactant, transition state and product structures along one of the two the proton transfer paths are shown on top for the three proton transfer processes.
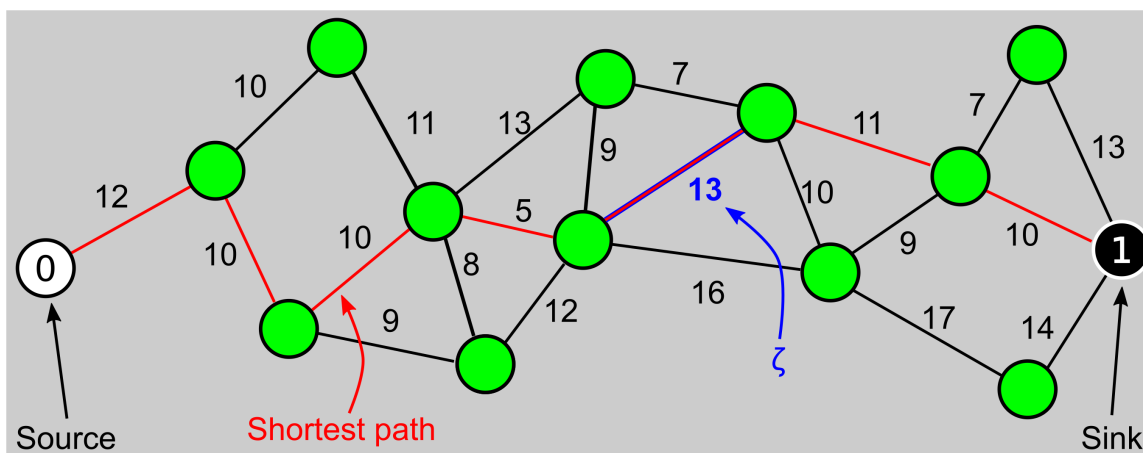
Figure S14. Longest connectivity, ζ (in blue), along the shortest path (red) for all possible pathways connecting the source (0; proton donor) to sink (1; proton acceptor). The shortest path was evaluated using Dijkstra's algorithm. Intermediate nodes in the graph (in green) represent proton-relaying species in a Grotthuss-type proton transfer process.

Table S1. Intrinsic proton affinities (in kcal mol^{-1}) of the protonatable groups in the BNC from DFT calculations. Geometries were optimized at BP86-D3/def2-SVP/def2-TZVP (Cu, Fe) level and the reported energies were obtained by performing single point calculations at B3LYP-D3/def2-TZVP level.

Proton acceptor\Redox state	P_R	$O_{H,R}$
Tyr-244	12.9	14.8
Heme a_3	1.0	9.7
Cu$_B$	21.3	-

Table S2. Employed protonation states in the MD simulations. All residues were modeled in their standard protonation states (Lys/Arg protonated; Glu/Asp deprotonated; His neutral, δ-tautomer) if not otherwise stated. HSE - neutral histidine ε-tautomer.

Protonated Lys-319 setup (Fig. 3, main text)
His-240 - neutral/HSE
Glu-242 - protonated OE2
Lys-319 - protonated
Asp-364 - protonated OD2
His-161 - neutral/HSE (subunit II)
His-204 - neutral/HSE (subunit II)

Deprotonated Lys-319 setup (ESI-Fig. 10)
His-240 - neutral/HSE
Glu-242 - protonated OE2
Lys-319 - deprotonated
Asp-364 - protonated OD2
His-161 - neutral/HSE (subunit II)
His-204 - neutral/HSE (subunit II)

References

[1]   T. Tsukihara, K. Shimokata, Y. Katayama, H. Shimada, K. Muramoto, H. Aoyama, M. Mochizuki, K. Shinzawa-Itoh, E. Yamashita, M. Yao, Y. Ishimura and S. Yoshikawa, *Proc. Natl. Acad. Sci. USA,* 2003, **100**, 15304–15309.

[2]   V. R. I. Kaila, M. I. Verkhovsky, G. Hummer and M. Wikström, *Proc. Natl. Acad. Sci. USA,* 2008, **105**, 6255–6259.

[3]   M. P. Johansson, V. R. I. Kaila and L. Laakkonen, *J. Comput. Chem.* 2008, **29**, 753–767.

[4]   A. D. MacKerell, D. Bashford, M. Bellott, R. L. Dunbrack, J. D. Evanseck, M. J. Field, S. Fischer, J. Gao, H. Guo, S. Ha, D. Joseph-McCarthy, L. Kuchnir, K. Kuczera, F. T. Lau, C. Mattos, S. Michnick, T. Ngo, D. T. Nguyen, B. Prodhom, W. E. Reiher, B. Roux, M. Schlenkrich, J. C. Smith, R. Stote, J. Straub, M. Watanabe, J. Wiorkiewicz-Kuczera, D. Yin and M. Karplus, *J. Phys. Chem. B,* 1998, **102**, 3586–3616.

[5]   J. C. Phillips, R. Braun, W. Wang, J. Gumbart, E. Tajkhorshid, E. Villa, C. Chipot, R. D. Skeel, L. Kale and K. Schulten, *J. Comput. Chem.,* 2005, **26**, 1781–1802.

[6]   W. Humphrey, A. Dalke and K. Schulten, *J. Mol. Graph.,* 1996, **14**, 33-38, 27–38.

[7]   S. Cukierman, *Biochim. Biophys. Acta* 2006, **1757**, 876–885.

[8]   D. Bashford and K. Gerwert, *J. Mol. Biol.,* 1992, **224**, 473–486.

[9]   G. Kieseritzky and E.W. Knapp, *Proteins: Struct*., *Funct*., *Bioinf*., 2008, **71**, 1335–1348.

[10]   B.K. Ho and F. Gruswitz, *BMC Struct. Biol. B,* 2008, **8**, 49.

[11]   J. P. Perdew, *Phys Rev B Condens Matter* 1986, **33**, 8822–8824.

[12]   A. D. Becke, *Phys Rev A,* 1988, **38**, 3098–3100

[13]   S. Grimme, *J. Comput. Chem.,* 2006, **27**, 1787–1799.

[14]   M. Sierka, A. Hogekamp and R. Ahlrichs, *J. Chem. Phys.,* 2003, **118**, 9136–9148.

[15]   F. Weigend and R. Ahlrichs, *Phys. Chem. Chem. Phys.,* 2005, **7**, 3297–3305.

[16]   A. Klamt and G. Schüürmann, *J. Chem. Soc., Perkin Trans.,* 1993, **2**, 799–805.

[17]   A. D. Becke, *J. Chem. Phys.,* 1993, **98**, 5648–5652.

[18]   R. Ahlrichs, M. Bär, M. Häser, H. Horn and C. Kölmel, *Chem. Phys. Lett.,* 1989, **162**, 165-169.

[19]   S. Riahi and C. N. Rowley, *J. Comput. Chem.,* 2014, **35**, 2076–2086.

[20]   S. Kumar, J. M. Rosenberg, D. Bouzida, R. H. Swendsen and P. A. Kollman, *J. Comput. Chem.,* 1992, **13**, 1011–1021.